Hindawi
Advances in Materials Science and Engineering
Volume 2019, Article ID 2382759, 8 pages
https://doi.org/10.1155/2019/2382759

Research Article

Failure Analysis on 42CrMo Steel Bolt Fracture

Guo Hongfei,[1,2] Jianwei Yan,[1,3] Ru Zhang,[1] Zhihui He,[1] Zengqi Zhao,[4] Ting Qu,[1] Ming Wan,[1] Jingshun Liu,[2] and Congdong Li[1]

[1]*Institute of Physical Internet, Jinan University, Zhuhai 519070, China*
[2]*School of Materials, Inner Mongolia University of Technology, Hohhot 010051, China*
[3]*State Key Laboratory for Strength and Vibration of Mechanical Structures, Xi'an Jiaotong University, Xi'an 710049, Shanxi, China*
[4]*Baotou Research Institute of Rare Earths, Baotou 014010, China*

Correspondence should be addressed to Jianwei Yan; tyanjianwei@jnu.edu.cn

Received 1 September 2018; Revised 12 October 2018; Accepted 17 October 2018; Published 1 January 2019

Guest Editor: Dariusz Rozumek

Fracture behaviors of 42CrMo ultrahigh strength steel-based bolt have been experimentally studied including macroscopic and microscopic fracture observation, metallographic test, mechanical property testing, and energy spectrum analysis. The results show that a large amount of structure defects, such as sulfide inclusions, band, and carbon depletion, appear in the fracture origin region and matrix of the bolt. Such defects reduce fatigue strength of materials and easily yields fatigue fracture origin. In addition, sulfide inclusions provide easy access to crack growth, gradually reducing the effective cross section of the bolt accompanying with increasing stress and finally causes fracture when stress exceeds the material fracture strength. The fracture mechanism is also explored based on fracture failure criterion and fatigue crack growth curve.

1. Introduction

The 42CrMo steel has been widely used as forgings due to its ultrahigh strength, toughness, good hardenability, unobvious temper brittleness, and higher fatigue limit and resistance to multiple impacts after quenching and tempering [1–3]. Such a kind of steel-based forgings possesses higher strength and larger quenching and tempering section, which are promising for the engineering applications in large gears for locomotive traction, rear axles of pressure vessels, extremely loaded connecting rod, spring clips, as well as deep well drill pipe joint and 2000 m underwater fishing tools.

However, malfunction inevitably occurs, and thus, a good understanding of the failure mechanism plays an important role in the optimized design and circumvented action. In this research work, macro-observations and micro-observations are carried out to analyze the mechanical behaviors and metallographic structure of bolt fracture origin region and matrix. In addition, by introducing fracture failure criterion [4, 5], the crack growth onset and direction analysis are theoretically explored, which provides a forecasting method and thus will be helpful in the engineering application.

The bolt is a fastening of the wind generator, with specification model of M30 × 435. The manufacturing process is described as follows: raw materials ⟶ fracturing materials ⟶ forging blanks ⟶ rough finish ⟶ heat treating ⟶ longitudinal mechanical property test ⟶ flaw detection ⟶ finish machining ⟶ finished products. When the bolt was installed and used, the customer found bolt fracture during routing inspection.

2. Test Process and Results

2.1. Macroscopic Observation of Fracture. The bolt fracture occurs at the position of 33 mm near the end of the bolt as shown in Figure 1. The bolt fracture is at the root of the thread. The morphology is as shown in Figure 2. Under macroscopic observation, obvious fatigue characteristics can be seen on the fracture. The fracture originates from the outer surface of the bolt. The fatigue origin area in the shape of semiellipse is relatively smooth. Clear fatigue lines can be

Figure 1: Macromorphology of fractured bolt.

Figure 2: Morphology of bolt fracture position.

observed in the extended area. The extended area covers most of the fracture, and the instantaneous fracture area is relatively small, with the morphology as shown in Figure 3. The surface of the bolt fracture is seriously worn out and shows different degrees of corrosion. The fracture morphology can no longer be observed. Based on the fracture morphology, instantaneous fracture area is close to the edge, indicating a low degree of bolt overload. If the bolt is a fracture caused by overload, the fiber zone is the location of the source of the fracture, and the fiber zone with the annular ridge pattern is always at the innermost volcano, not the edge.

2.2. Mechanical Property Test of Bolt Matrix. A set of tensile specimens and three impact specimens are taken on the fracture bolt for the mechanical property test, as shown in Table 1.

As shown in Table 1, the mechanical property of the fractured bolt meets the technical requirements of GB/T3077.

2.3. Metallographic Test of Bolt Matrix. Tests of nonmetallic inclusions, microstructure, and grain size have been conducted by sampling on bolt matrix. The metallographic test results are as shown in Table 2. The structure morphology is as shown in Figure 4, and the grain size is as shown in Figure 5.

As shown in Table 2, no obvious abnormality is observed in the test results of nonmetallic inclusions, microstructure, and grain size of this bolt.

2.4. Fracture Observation with a Scanning Electron Microscope and Energy Spectrum Analysis. Clean the bolt fracture with an ultrasonic oscillator, and observe microscopic fracture morphology with a scanning electron microscope (FEG-450). It is found that microscopic fracture of the bolt is severely scratched and rusted, and the fracture morphology cannot be clearly observed. However, a large number of

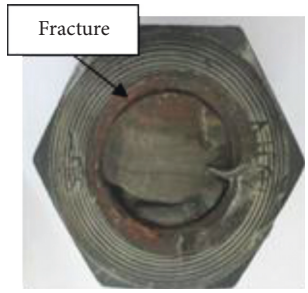

Figure 3: Morphology of bolt fracture.

Table 1: Results of mechanical property test.

Test result	RP0.2 (MPa)	Rm (MPa)	A (%)	Z (%)	Impact test result KV2 (J)	HRC
GB/T3077 (standard value)	≥930	≥1080	≥12	≥45	≥63	32–38
Test value	1055	1127	16.5	56	−20°C: 63.7 70.4 71.3	36.0

Table 2: The results of the metallographic test.

Bolt	Nonmetallic inclusions (level)	Microstructure	Grain size (level)
/	A2.0; B0; C0; D0.5e; DS1.0	Tempered sorbite + small amounts of bainite	8.5
Test standard	GB/T10561-2005	GB/T13298-1991	GB/T6394-2002

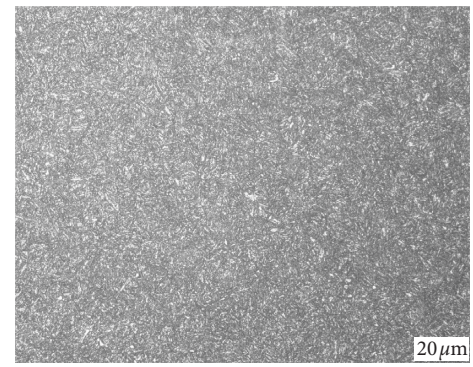

Figure 4: Metallographic structure of bolt matrix.

holes are observed in the fracture origin area (Figure 6). Less obvious fatigue striations are distributed in the extended area, with the morphology as shown in Figure 7. Under magnified observation, the fracture surface is relatively flat and a large number of secondary cracks are distributed on the fracture surface, with the morphology as shown in Figure 8. According to the semiquantitative analysis of energy spectrum performed on the gray products in the crack of metallographic specimen, the crack mainly contains elements including Os, Cr, Mn, and Fe. See Figure 9 for the energy spectrum.

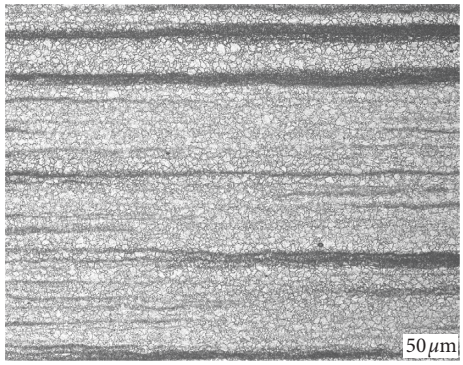

Figure 5: Grain size of bolt matrix.

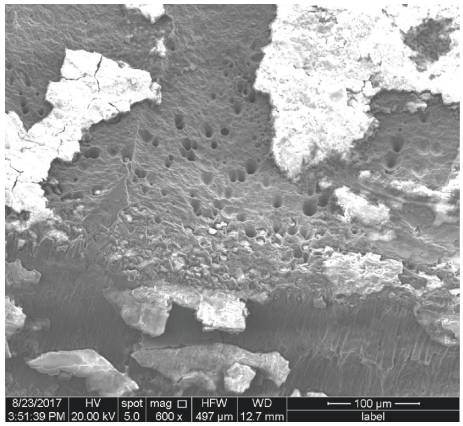

Figure 6: Micromorphology of fracture origin area.

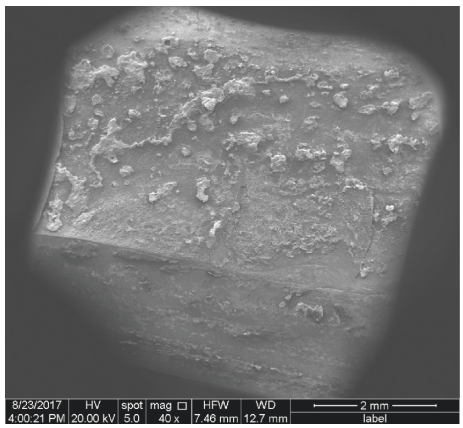

Figure 7: Micromorphology of fracture extended area.

According to the above results of electron microscopy and energy spectrum, it is known that there are a large number of hole defects in the fracture source region, which is the direct cause of the fracture of the whole bolt. The fatigue fringe distributed in the extended region is one of the important microscopic bases for the fatigue fracture of the part, because fatigue streaks appear in the second stage of fatigue crack propagation, where the crack growth rate is faster, and each stress cycle is on the order of microns. The gray product of the crack mouth is the oxidation product, and the crack

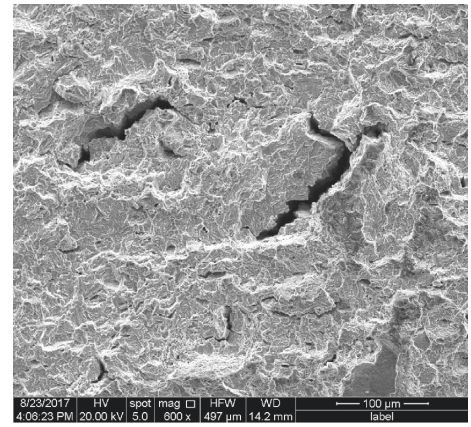

Figure 8: Macromorphology of secondary fracture crack.

tail is the manganese sulfide inclusion. The existence of these structures destroys the continuity of the surface of the material, causing the formation of cracks in the Hertz region of the subsurface, and especially the brittle oxide and the matrix are separated into voids. The stress concentration at the sharp corners of the cavity edges exceeds the elastic limit of the matrix, and the plastic deformation is large, causing the surface of the material to harden, thereby causing cracks.

2.5. Microscopic Observation of Fracture Origin. Cut the bolt at the fracture origin area longitudinally and grind it. Under the metalloscope, many small cracks extending from the fracture to the matrix can be observed. The deepest crack depth measures 0.10 mm, with the morphology shown in Figure 10. Under magnified observation, the cracks are filled with gray products (Figure 11). Concentratedly distributed manganese sulfide inclusions are found near the fracture origin (Figure 12). Many manganese sulfide inclusions are also observed in the matrix.

Upon corrosion of the sample in 4% nitric acid alcohol solution, carbon depletion is observed at the fracture origin. The deepest depth of the carbon-depleted layer is 0.40 mm, with the morphology shown in Figure 13. At the fracture origin, bands are distributed in the same direction as the crack propagation, and some microcracks extend along the banded structure, with the morphology as shown in Figure 14. Bands are also distributed in the matrix. According to GB/T13299-1991, the banded structure is rated as 3C2.5, with the morphology as shown in Figure 15. Carbon depletion is observed at addendum and both tooth sides of the bolt, with the morphology as shown in Figure 16.

It can be seen from the above microscopic results that the deepest crack depth in the fracture source region is 0.10 mm, and the crack initiation phase is 0.05–0.08 mm in the engineering. It is known that the deepest crack in the fracture source region has crossed the crack initiation stage to reach the crack. During the expansion phase, the presence of cracks causes stress and strain concentration on the surface of the bolt, forming a fatigue source at the crack and accelerating the initiation and propagation of fatigue cracks. There is carbon depletion at the source of the fracture, the

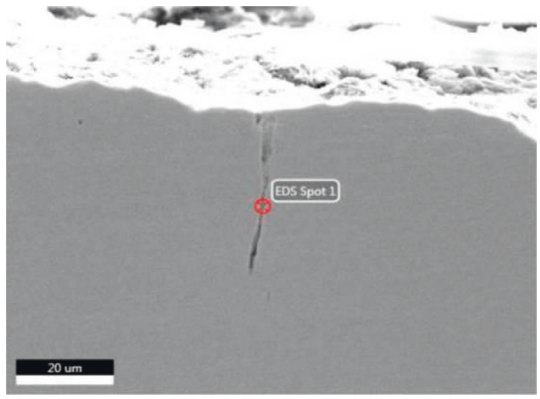

eZAF intelligent quantitative

Element	Weight %	Atom	Net	Error %
O K	2.71	8.45	65.18	11.45
S K	6.41	9.99	351.15	5.44
CrK	1.21	1.16	50.67	13.14
MnK	11.5	10.46	293.65	3.42
FeK	78.17	69.93	1665.52	1.92

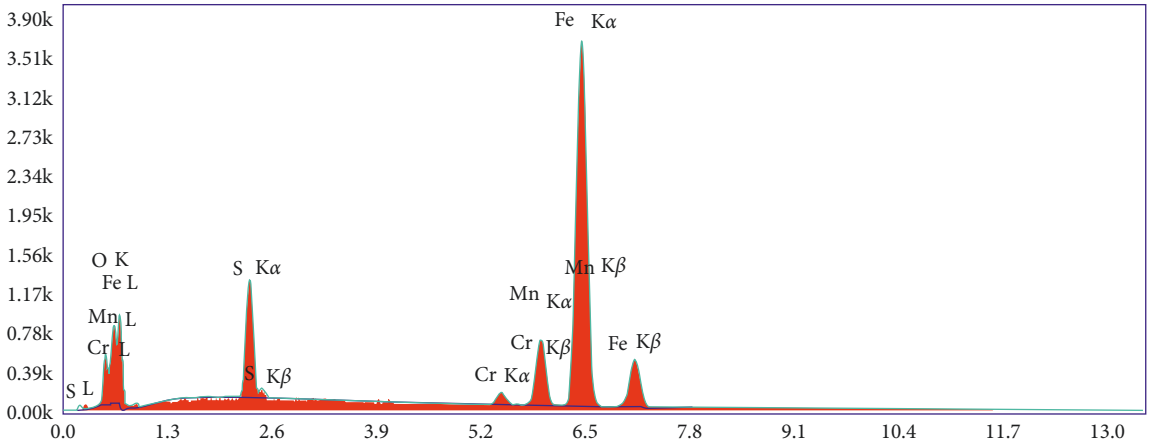

Figure 9: Energy spectrum.

Figure 10: Micromorphology of small cracks.

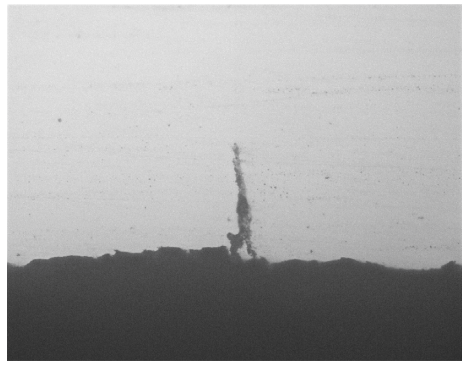

Figure 11: Magnified micromorphology of small distributed cracks in fracture origin area.

root of the bolt, and the sides of the tooth. The carbon depletion is partial decarburization. The decarburization causes the surface hardness to decrease; thus the yield strength of the material decreases and the plastic deformation is easy. The increase of surface friction coefficient promotes the formation of surface cracks. Defects in the band structure at the source of the fracture and in the matrix are also one of the causes of fatigue fracture. Due to the different microstructures of the adjacent bands of the banded structure, their properties are also different. The bands with low performance under external force are easily exposed, and stress concentration occurs between the strong and weak bands, thus causing a decrease in overall mechanical properties. There is obvious anisotropy, thus reducing the fatigue properties of materials.

3. Fracture Failure Criterion

For brittle fracture of homogeneous materials, take the stress intensity factor and energy release rate as the crack propagation forces and fracture toughness as the fracture resistance parameter [6, 7]. Assuming that the energy release rate (G) reaches the fracture toughness of the material (Γ),

Figure 12: Micromorphology of nonmetallic.

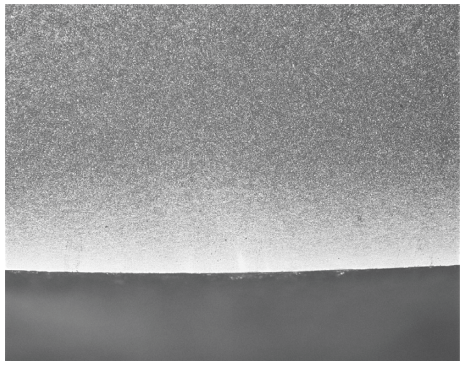

Figure 13: Micromorphology of carbon inclusions near the fracture surface depletion near the fracture origin.

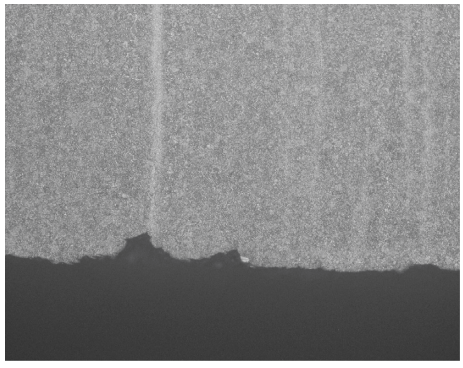

Figure 14: Micromorphology of the band.

the crack begins to grow. G is the function of K_{II}/K_I, crack propagation angle φ (angle between the crack propagation direction and the positive direction of the X axis $-\pi < \Phi < \pi$), external load, and elastic modulus. The fracture criterion can be expressed as

$$G = \Gamma, \qquad \frac{\partial(G - \Gamma)}{\partial \Phi} = 0. \tag{1}$$

If the toughness value of the material in $\Phi \neq 0$ direction is greater than that in $F = 0$ direction, the fracture criterion can be expressed as

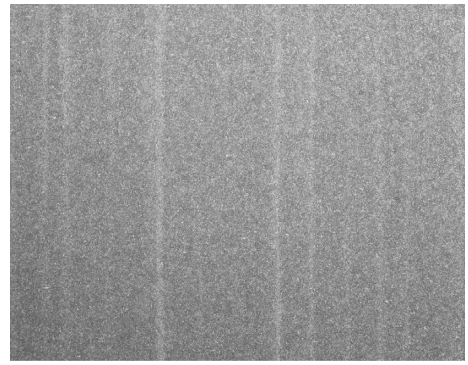

Figure 15: Micromorphology of the matrix band at the fracture origin.

$$G = \Gamma, \tag{2}$$

where Γ is a toughness value along $\Phi = 0$, obtained by the test and methods of mesomechanics. Based on the study of Gu and Asaro [8, 9] and the analysis on specimens of in-plane and antisymmetric loads, the following can be suggested:

(1) The greater the material nonuniformity, the larger the type II stress intensity factor. The crack propagates in the direction in which the difference in energy release rate and fracture toughness is the greatest.

(2) When the crack is located in the center of the specimen, the nonuniformity of the material has a great effect on the direction of crack propagation, and when the crack is close to the boundary of the specimen, the nonuniformity has little effect on it.

4. Mechanism Analysis and Discussion

The above test results suggest that the mechanical property of the bolt conforms to the technical requirements of GB/T3077 and the metallographic structure is a normal quenched and tempered structure. Under microscopic observation, the bolt has structural defects of many sulfide inclusions, indicating that the material has poor desulfurization in the desulfurization process. Meanwhile, fine cracks extending from the outer surface into the matrix are observed in the fracture origin area of the bolt. The cracks are filled with gray products. Based on the electron microscope and energy spectrum analysis, the gray products in the front part of the crack are oxidation products, and those in the rear part of the crack are manganese sulfide inclusions. Nonmetallic inclusions in steel, especially oxides, are coarse and unevenly distributed and are not deformed in a point shape, which greatly reduces the fatigue wear resistance of the material. Although the sulfide is less harmful than the oxide, if the sulfide content in the steel is high, the continuity of the surface of the material is also destroyed. This is because the sulfide has plasticity in the hot working state and the expansion coefficient is close to that of the steel, which is deformed together with the matrix. Fatigue crack sources are often generated in areas

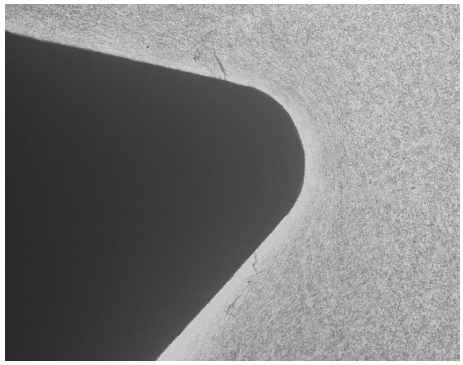

Figure 16: Micromorphology of carbon depletion at addendum and both tooth sides of the bolt.

with severe defects and stress concentrations. Therefore, in use, the bolt forms a stress concentration point at the hole and the inclusion defect in the fracture source region and then becomes a crack source. In the subsequent use, the crack further extends and expands and finally causes the bolt to be unstable and fractured.

The banded structure of the bolt is obvious, and the grow direction of the banded structure is consistent with the direction of crack propagation. The banded structure includes a primary banded structure and a secondary banded structure. The primary band structure is the original band shape, which is caused by the dendrite segregation generated when the steel ingot is cast; the secondary band structure is formed on the basis of the primary strip shape, which is generated along the rolling direction of the steel after rolling or heat treatment. The eutectoid ferrite band and the pearlite band are stacked on each other in a band structure. The secondary band structure can be alleviated or eliminated by a reasonable heat treatment process, and the primary band structure is difficult to be eliminated by common heat treatment. However, it is difficult to eliminate the primary banded structure by common heat treatment, which needs to be avoided or improved by electroslag remelting, liquid steel crystallization speed increasing, final rolling (forging) temperature increasing, forging ratio increasing or diffusion annealing, and other technologies. The presence of banded structure causes two structural stress differences and material anisotropy, providing a convenient channel for crack propagation.

There is carbon depletion at the source of bolt breakage, the root of the tooth, and both sides of the tooth. Although the carbon-poor layer is very shallow, only 0.40 mm, even negligible for large-size shafts, in practice the thin-layer decarburization of the surface is a fatal defect. Decarburization is a fatal flaw, and decarburization of 0.1 mm will significantly reduce the fatigue limit. In addition, the presence of the decarburization layer reduces the fatigue strength of the surface of the part. Under the action of alternating stress in the long-term use, the surface has fatigue cracks, and the existence of fatigue cracks causes stress concentration in the source region, also in actual use. If subjected to a large impact force, the crack will develop rapidly, causing the bolt to break.

The crack originates at the bottom of the first thread, and deformation mark is observed on the thread surface. This mark should be formed during the process of pretightening the bolt. The morphology of the bolt fracture indicates that the crack initiation stress is large. In this aspect, it also shows that the bolt was subjected to pretightening force. Pretightening force refers to tightening force, which is also the shear stress [10–12]. Tensile load is the main work load. Pretightening force overlapping with service stress promotes the crack initiation. When the crack origin appears on the surface, the fatigue crack origin develops based on the microcrack nucleation [13–16]. These microcracks gradually and progressively grow with the repeated stress. When the fatigue cracks grow to a certain extent, the effective cross section of the part is greatly reduced while the stress is continuously increased. When the stress exceeds the fracture strength of the material, the fracture occurs.

According to the fracture criterion, when the energy release rate (G) of the homogeneous material reaches the fracture toughness of the material (Γ), the crack begins to grow. Corresponding to the crack initiation stage when the crack depth is 0.05–0.08 mm, it provides a theoretical basis for predicting the timing of crack initiation. The greater the nonuniformity of the material, the larger the stress intensity factor of type II, and the crack expands along the direction of the difference between the energy release rate and the fracture toughness. However, there are many structural defects in the fracture bolt, which leads to poor uniformity of the material. That is, the material nonuniformity is large, and the type II stress intensity factor is large, causing the crack to start cracking along the defects such as inclusions. When the crack is located in the center of the test piece, the material nonuniformity has a great influence on the direction of crack propagation. When the crack is close to the boundary of the test piece, the nonuniformity has little effect on the crack propagation direction and the fracture position of the bolt test piece in this paper. The fracture position of the bolt specimen is at the root of the thread; that is, the crack is close to the boundary of the specimen, so the nonuniformity of the material has little influence on the crack propagation direction.

In summary, the fracture property of the fault bolt is a typical fatigue fracture, involving three stages: crack initiation, crack propagation, and instantaneous fracture. The typical fatigue crack growth curve is shown in Figure 17. The three general causes of crack initiation are surface roughness due to slip band; crack source formed in the grain boundary due to serious misalignment of the strain; and surface inclusions, processing defects, and nucleation of the chemical segregation area. For the bolt in this paper, crack initiation is caused by surface inclusions, processing defects, and nucleation of the chemical segregation area. For industrial materials, defect areas involving inclusions, voids, surface processing defects, and microarea of chemical segregation can also become sites of fatigue crack initiation [17–19]. The mechanism of fatigue crack initiation at the defect site is related to a series of mechanical factors, microstructure factors, and environmental factors [20–23]. These factors include the slip characteristics of matrix, the relative strength of matrix and defect, the strength of matrix and inclusion

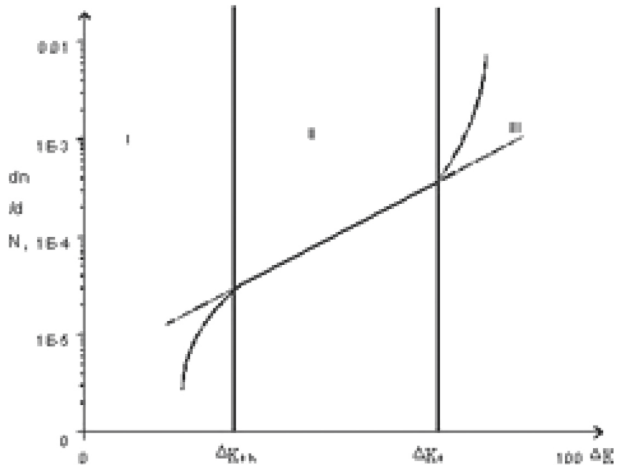

Figure 17: Typical fatigue crack growth curve.

interface, and the relative sensitivity of matrix and inclusions to corrosion in a fatigue environment. The fatigue submicroscopic cracks formed in the metal connect to form microscopic fatigue cracks [24, 25], which is called the first stage of crack formation. Then, the cracks continue to grow in the direction of the maximum shear stress that forms an angle of about 45° with the load, which is the second stage of fatigue crack formation. When the crack propagates perpendicular to the load direction, the normal stress has a great influence on the crack propagation and the crack propagation speed and depth are much greater than before. When the crack propagates to a certain critical length, the instability expansion causes rapid fracture.

5. Conclusions

(1) Based on macroscopic and microscopic observation and analysis of the fractured bolt, the bolt fracture is determined as a fatigue fracture.

(2) The mechanical property and the matrix microstructure of the bolt meet the technical requirements.

(3) The fracture origin area and matrix of the bolt involve structure defects including a large amount of sulfide inclusions, segregation, and carbon depletion. The presence of defects reduces the fatigue strength of the material, and fatigue fracture origin is easily formed in the weak area of the material. Cracks continue to grow along the sulfide inclusions and gradually reduce the effective crosssection of the bolt while the stress increases. When the stress exceeds the fracture strength of the material, the fracture occurs.

Data Availability

The data used to support the findings of this study are available from the corresponding author upon request.

Conflicts of Interest

The authors declare that there are no conflicts of interest regarding the publication of this paper.

Acknowledgments

The research and publication of this article was supported by the Fundamental Research Funds for the Central Universities (No. 21618412), Inner Mongolia Autonomous Region Science and Technology Innovation Guide Award Fund Project (No. 103-413193), and Open Project of Key Laboratory for Strength and Vibration of Mechanical Structures (SV2017-KF-23).

Supplementary Materials

The Supplementary Materials contain all the original images of the paper. (*Supplementary Materials*)

References

[1] Z. Yu, P. Jiang, Z. Yao, and Y. Xu, "Fracture analysis of bolt made of 42CrMo steel," *Heat Treatment of Metals*, vol. 37, no. 4, pp. 134–136, 2012.

[2] Y. Xiong, C. Chen, X. Xie et al., "42CrMo steel bolt failure analysis," *Aerospace Materials and Technology*, vol. 47, no. 3, pp. 67–70, 2017.

[3] S. Gao, Y. Xu, G. Sun, and J. Zhang, "Fracture analysis of high strength bolt," *Physical Testing and Chemical Analysis Part A: Physical Testing*, vol. 42, no. 6, pp. 306–308, 2006.

[4] D. Yao, X. Yan, M. Chen, and J. He, "Elastic fracture mechanics analysis of functionally gradient materials," *Rare Metal Materials and Engineering*, vol. 34, no. 8, pp. 1191–1195, 2005.

[5] D. Zhang, P. Zhong, C. Tao et al., *Failure Analysis*, National Defend Industry Press, Beijing, China, 2004.

[6] Z. Wang, *Fatigue of Materials*, National Defense Industry Press, Beijing, China, 1993.

[7] C. Chen, *Fatigue and Fracture*, Huazhong University of Science and Technology Press, Wuhan, China, 2002.

[8] P. Gu and R. J. Asaro, "Cracks in functionally graded materials," *International Journal of Solids and Structures*, vol. 34, no. 1, pp. 1–17, 1997.

[9] P. Gu and R. J. Asaro, "Crack deflection in functionally graded materials," *International Journal of Solids and Structures*, vol. 34, no. 24, p. 3085, 1997.

[10] T. Zhang, Z. Zhao, L. Ni, and X. Xue, "Fracture failure analysis of hexagon head bolt," *Metal Products*, vol. 42, no. 4, pp. 719–721, 2016.

[11] C. Hu, X. Liu, C. Tao et al., "Failure analysis on 0Cr17Ni4-Cu4Nb screw," *Journal of Materials Engineering*, vol. 12, pp. 21–23, 2012.

[12] C. Hu, T. Jiang, and X. Liu, "Failure analysis of steel screws," *Heat Treatment of Metals*, no. 2, pp. 141–144, 2014.

[13] Z. Han, H. Ma, and Y. Ding, "Fracture failure analysis of the high strength bolt," *Physical Testing and Chemical Analysis (Part A: Physical Testing)*, vol. 39, no. 9, pp. 477–480, 2003.

[14] T. Zhou and J. Suo, "Failure analysis on 42CrMo steel connecting rod," *Chemical Engineering and Equipment*, no. 4, pp. 21–24, 2016.

[15] W. Jiang, J. Gong, and S. Tu, "Analysis of fatigue fracture mechanism for brazed 304 stain-less steel plate-fin structure," *Transactions of the China Welding Institution*, vol. 31, no. 4, pp. 45–48, 2010.

[16] L. Jiang, J. Zhang, S. Zhang et al., "High-cycle fatigue fracture mechanism for ZTC4 alloy," *Hot Working Technology*, vol. 42, no. 10, pp. 93–95, 2013.

[17] M. Endo and A. J. McEvily, "An analysis of the fatigue strength of metals containing small defects," *Key Engineering Materials*, vol. 353–358, pp. 323–326, 2007.

[18] W. C. Cui and X. P. Huang, "A general constitutive relation for fatigue crack growth analysis of metal structures," *Acta Metallurgica Sinica*, vol. 16, no. 5, pp. 342–354, 2003.

[19] M. D. Chapetti, T. Tagawa, and T. Miyata, "Ultra-long cycle fatigue of high-strength carbon steels part I: review and analysis of the mechanism of failure," *Materials Science and Engineering: A*, vol. 356, no. 1-2, pp. 227–235, 2003.

[20] X. Huang, G. Jia, W. Cui et al., "Unique crack growth rate curve model for fatigue life prediction of marine steel structures," *Journal of Ship Mechanics*, vol. 15, no. 1, pp. 118–125, 2011.

[21] F. Wang, W. Cui, and X. Huang, "Evaluation of surface crack shape evolution using the improved fatigue crack growth rate model," *Journal of Ship Mechanics*, vol. 15, no. 6, pp. 660–668, 2011.

[22] C. Santus and D. Taylor, "Physically short crack propagation in metals during high cycle fatigue," *International Journal of Fatigue*, vol. 31, no. 8-9, pp. 1356–1365, 2009.

[23] K. Wang, F. Wang, W. C. Cui et al., "Prediction of short fatigue crack growth life by unified fatigue life prediction method," *Chuan Bo LI Xue/Journal of Ship Mechanics*, vol. 18, no. 6, pp. 678–689, 2014.

[24] A. Abdullah, H. Alfawaz, Amani bin Rabba, A. Almutairi, S. Alnafaiy, and M. K. Mohammed, "Failure analysis and reliability of Ni–Ti-based dental rotary files subjected to cyclic fatigue," *Metals*, vol. 8, no. 1, p. 36, 2018.

[25] J. Ina, M. Vallentyne, F. Hamandi et al., "Failure analysis of PHILOS plate construct used for pantalar arthrodesis paper I—analysis of the plate," *Metals*, vol. 8, no. 3, p. 180, 2018.